Applied Physics A (2020) 126:171
https://doi.org/10.1007/s00339-020-3340-z

Applied Physics A
Materials Science & Processing

Low-frequency dielectric processes in deformed helix ferroelectric liquid crystals

Ambika Bawa[1,4] · Amit Choudhary[2] · Anil K. Thakur[3] · Suraj Kumar[4] · Rajesh[1,4] · Surinder P. Singh[4] · Ashok M. Biradar[4]

Received: 30 October 2019 / Accepted: 25 January 2020 / Published online: 10 February 2020

Abstract
A low-frequency dielectric relaxation mode in deformed helix ferroelectric liquid crystal (DHFLC) has been observed at the interface of strongly rubbed substrates and DHFLC material which may find applications in low power consumption FLC devices. The surface-induced dielectric relaxation process at the interface of DHFLC and substrate is called the partially unwound helical mode (*p*-UHM) due to the unwinding of the helical structure at this interface. After investigation of the material under various parameters such as temperature, variation of the amplitude of probing ac voltage and dc bias voltage, the relaxation frequency of *p*-UHM is found to be shifted towards Goldstone mode and merged with it. The relaxation frequency of Goldstone mode is found to decrease, whereas the relaxation frequency of *p*-UHM process increases with the increase in temperature of DHFLC. Finally, both the modes merge and the resultant relaxation frequency is found to be lower than Goldstone mode in SmC* phase. It seems that phason mode and partial helical unwinding mode are coupled together due to dipole moment that is resulting in a new relaxation frequency. *p*-UHM process is significant for low-power displays and non-displays applications like a part of sensor where weak electric signal is required to be realized without pre-amplification.

Keywords Deformed helix ferroelectric liquid crystal · Dielectric spectroscopy · Surface interface

1 Introduction

Ferroelectric liquid crystals (FLCs) have been investigated a lot due to their applied and basic aspects. As far as basic aspects are concerned, there have been some dynamical processes in which the focus needs to be concentrated as it could give wider practical applications of FLC materials. Some of the significant aspects were the gray scale phenomenon in deformed helix FLC (DHFLC) invented by Beresnev et al. [1], where the pitch value of FLC material was very small (< 1 μm). As far as the applied aspects are concerned, many research papers are published in DHFLC materials such as spatial light modulators [2], polarization grating, [3] optical bistability, [4, 5] and incorporation of nanomaterials in DHFLCs [6–8]. To understand the phenomenon in FLCs, different dielectric modes have been observed such as Goldstone mode, soft mode, unwound helical mode [9, 10], domain mode observed by Haase's group [11], where in high spontaneous polarization (P_s) FLCs, the helix is found splitted near the surface and the bulk material which form the domains.

The helical unwinding process has a great significance because the unwinding of helical structure leads to the molecular switching process resulting into some changes in material properties that lead to their practical applications. The unwinding of helix by electric field was proposed by Meyer in 1970 [12] by giving its similarity with helical unwinding process in cholesteric liquid crystals [13]. The method of helical unwinding had also been reported by shear flow [14], but not used frequently in case of FLCs. The helical dynamic process in FLCs had

✉ Amit Choudhary
amitnpl2005@gmail.com

✉ Ashok M. Biradar
abiradar.npl@gmail.com

[1] Academy of Scientific and Innovative Research (AcSIR), Gaziabad 201002, India

[2] Physics Department, Deshbandhu College (University of Delhi), Kalkaji, New Delhi 110019, India

[3] Department of Nano Science and Materials, Central University of Jammu, Jammu 180011, India

[4] CSIR-National Physical Laboratory, Dr. K. S. Krishnan Marg, New Delhi 110012, India

been investigated by several techniques such as electro-optical [10], conoscopy [15] and dielectric spectroscopy [11]. The helical unwinding and winding process leads to the two dielectric relaxation processes. The unwinding process was faster than the winding process at low frequency of 10 Hz. The unwinding process was achieved by the application of external electric field, while the winding process takes longer time as it depends on the natural winding of the helix and was dependent on the viscosity of the FLC material [16]. On the other hand, the V-shaped electro-optical switching of DHFLC showed almost no difference in two processes at higher frequencies 500 Hz and 2 kHz [17]. The helical unwinding process had been explored theoretically under the fixed boundary conditions of the sample cell and found to be dependent on the boundary conditions [18]. It was shown theoretically that the unwinding of helix takes place at a critical thickness of sample cell. The thickness of the cell was found to affect the saturation of polarization and the critical field of helical unwinding. Furthermore, the helical unwinding by surface effect boundaries in cell of different thicknesses had shown the contribution to effective dielectric susceptibility due to the occurrence of anisotropy of susceptibility in the plane perpendicular to the helical axis [19].

A lot of research work had been done on DHFLCs and FLCs [20–26], related to dynamics of helix behavior. Recently, a dielectric relaxation process was observed at a lower frequency than Goldstone mode frequency in DHFLC and conventional FLC materials, called as partially unwound helical mode (*p*-UHM) [27]. The helix of the DHFLC was unwound partially by strong rubbing repetitions effect of the nylon 6/6-coated substrate. It was shown experimentally in these sample cells that the amplitude of probing ac voltage shifts the relaxation frequency of *p*-UHM towards higher frequency and finally merges with Goldstone mode. The behavior of Goldstone mode relaxation frequency was dominated by this *p*-UHM when it was close to the Goldstone mode frequency. This resulted in the shifting of Goldstone mode relaxation frequency towards lower side and it merges with *p*-UHM process [28].

In present investigations, the behavior of *p*-UHM has been studied as a function of temperature in chiral smectic C (SmC*) of DHFLC in the large number (40) of repetitions of nylon 6/6-coated substrate of the sample cell. It has been observed that there is a strong correlation between *p*-UHM and Goldstone mode. The relaxation frequencies of the *p*-UHM and Goldstone mode have been observed to merge together resulting in to a single relaxation process. The permittivity of the DHFLC sample at high amplitude of probing ac voltage has been found to be highly influenced by *p*-UHM in SmC* phase in DHFLC material. The study signifies the behavior of DHFLC material throughout the SmC* phase under the influence of *p*-UHM process.

2 Experimental

2.1 Substrate preparation and characterization

The highly conducting (~ 20 Ω/□) indium tin oxide (ITO)-coated glass plates were used to prepare the sample cells. The desired electrode pattern of ITO on glass substrate was prepared using photolithography technique and the active electrode area was 0.4 cm × 0.4 cm. The planar alignment of FLC molecules in the cells was achieved by rubbing the nylon 6/6-coated glass substrate using velvet cloth.

For the realization of weakly and strongly rubbed surfaces, four types of substrate surfaces were prepared and optimized by contact angle and atomic force microscopy (AFM) techniques as shown in Fig. 1. As can be seen from the Fig. 1a–c, the increase in the number of grooves formation was visualized till ten repetitions of rubbing and showed a continuous increase in the corresponding contact angle of water. But as the number of rubbing repetitions was further increased beyond 40 repetitions, the grooves visualization was found to be reduced and the contact angle was found increasing slowly which indicates towards the little modification in the surface morphology. The large number of repetitions induces the roughness. It is also predicted that the large number of repetitions induces and aligns the polymer chains, and gives better alignment of FLCs molecules [29–32]. Therefore in the present investigation, the surfaces with rubbing repetitions of 10 and 40 were considered as weakly and strongly rubbed polymer surfaces for the sample cells, respectively.

2.2 Cell fabrication

The thickness of the sample cell was maintained by Mylar spacers (~ 8 μm). The DHFLC material was filled in its isotropic phase by means of capillary action and then cooled gradually to room temperature. The phase sequence of the deformed helix FLC material, LAHS-2 [33] is as

$$\text{Cryst.} \overset{?}{\leftrightarrow} \text{SmC}* \overset{58^{\circ}\text{C}}{\leftrightarrow} \text{SmA} \overset{62.5^{\circ}\text{C}}{\leftrightarrow} \text{Iso.}$$

The pitch value of the material was observed around ~ 0.4 μm.

2.3 Instrumentation

The planar alignment was checked under the polarizing optical microscope (Axioskop-40, Carl Zeiss, Germany). The dielectric studies of the material were done using an impedance analyzer (Wayne Kerr 6540A, frequency range 20 Hz–120 MHz, UK) in the frequency range

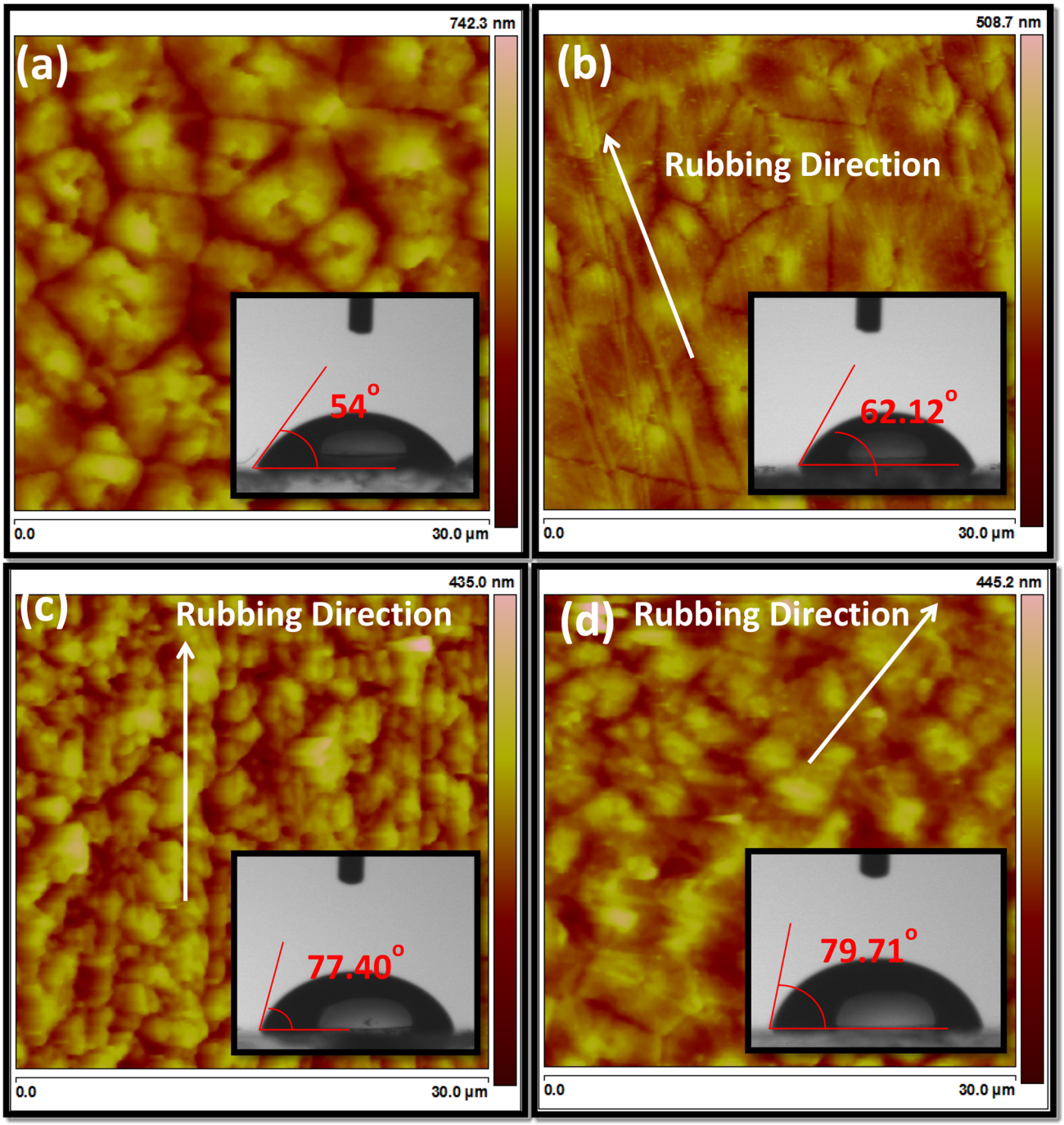

Fig. 1 Characterization of nylon 6/6 polymer alignment layer in various rubbing conditions using atomic force microscopy and contact angle of water measurement **a** no rubbing, **b** 3, **c** 10, and **d** 40 repetitions of rubbing. Inset images show the contact angle of water on corresponding rubbed configuration of nylon 6/6 polymer alignment layer on the glass substrates

of 20 Hz–1 MHz. The temperature of the sample cell was controlled through the sample holder using temperature controller (Julabo, Germany) with an accuracy of ± 0.1 °C. The dielectric studies were carried out at different temperatures and at various applied probing ac voltage from 100 mV to 700 V in the frequency range of 20 Hz–1 MHz. The optical transmission spectra were recorded in UV–visible range using UV–visible spectrophotometer (Agilent, Cary 5000 UV–Vis–NIR, USA).

3 Results and discussion

3.1 Theoretical formulation for data fitting

The combination of two relaxation processes is found to conform Cole–Cole model [34] of dielectric spectroscopy in SmC* phase of deformed helix FLC [35]

$$\varepsilon^* = \varepsilon' - i\varepsilon'' = \varepsilon_\infty + \sum_j \frac{\Delta\varepsilon_j}{1 + \left(i\omega\tau_j\right)^{(1-\alpha_j)}} + \frac{\sigma}{i\omega\varepsilon_o}. \quad (1)$$

Here, j stands for number of dielectric relaxation processes in the deformed helix FLC material. In the present system, we have observed two relaxation processes: one is Goldstone mode and another is p-UHM. Therefore, j can be extended up to 2 i.e., $j = 1$ (Goldstone mode) and 2 (p-UHM). This means the net permittivity is the contribution of two relaxation processes.

The real and imaginary parts of the Eq. (1) are:

$$\varepsilon' = \varepsilon_\infty + \sum_{j=1,2} \frac{1}{2}\Delta\varepsilon_j \left\{ \frac{1 + \left(\omega\tau_j\right)^{1-\alpha_j} \sin\left(\pi\alpha_j/2\right)}{1 + 2\left(\omega\tau_j\right)^{1-\alpha_j} \sin\left(\pi\alpha_j/2\right) + \left(\omega\tau_j\right)^{2(1-\alpha_j)}} \right\}, \text{ and} \quad (2)$$

$$\varepsilon'' = \sum_{j=1,2} \frac{1}{2}\Delta\varepsilon_j \left\{ \frac{1 + \left(\omega\tau_o\right)^{1-\alpha_j} \cos\left(\pi\alpha_j/2\right)}{1 + 2\left(\omega\tau_j\right)^{1-\alpha_j} \sin\left(\pi\alpha_j/2\right) + \left(\omega\tau_j\right)^{2(1-\alpha_j)}} \right\} + \frac{\sigma_{dc}}{\epsilon_o\omega}, \quad (3)$$

respectively.

$$\Delta\varepsilon_j = \varepsilon_{jo} - \varepsilon_\infty, \quad (4)$$

where ε_{jo} and ε_∞ are the permittivity of a particular process at low frequency and the permittivity at high frequency, respectively.

The $\omega(= 2\pi\nu)$ is angular frequency of the applied electric field. Here, ν is the linear frequency of applied field. Also, ε_∞, $\Delta\varepsilon_1$ and $\Delta\varepsilon_2$ are the permittivity at high frequency, dielectric strength of relaxation process of Goldstone mode and p-UHM, respectively. ω is the angular frequency. τ_1 and τ_2 are the relaxation time of the Goldstone mode and p-UHM, respectively. α_1 and α_2 are the distribution functions of Goldstone mode and p-UHM, respectively. $\sigma(\sim 1.9 \times 10^{-9}$ S/m) is the dc ionic conductivity and ε_o is the permittivity of free space.

3.2 Effect of temperature on dielectric properties

It is well known that the collective dielectric processes in SmC* phases were mainly due to phase and tilt angle fluctuations, called as Goldstone and soft modes in planar alignment [36, 37]. These two modes were observed and reported almost in all type of FLCs. The Goldstone mode or the phason mode (ϕ, fluctuations) appeared throughout the SmC* phase. Most of the permittivity values in SmC* phase at lower frequencies were dominated by Goldstone mode and therefore, other relaxation processes were masked by Goldstone mode. Generally, in SmC* phase of FLCs, the permittivity value for lower frequency (~ 100 Hz) is very large than the permittivity at higher frequency (~ 100 kHz). This higher value of permittivity at ~ 100 Hz is due to the contribution from Goldstone mode. Figure 2 shows the real (ε') and imaginary (ε'') parts of complex permittivity (ε*) at different temperatures in SmC* phase at 100-mV probing ac voltage. As seen in Fig. 2a, the permittivity (ε') at room temperature is around 60 at 20-Hz frequency and as the temperature increases, it reaches 200 at 55.5 °C, which is a large jump in the ε' value at 100 mV probing ac voltage. As one can see in Fig. 2a, the ε' first increases with temperature from 30 to 55.5 °C below T_c temperature and then starts decreasing with temperature at 100-mV probing ac voltage in SmC* phase of DHFLC material. The peak frequency of ε'' (Goldstone mode relaxation process), first decreases upto 55.5 °C and then increases with temperature Fig. 2b. Similar type of behavior of relaxation peak frequency in tanδ vs frequency response has been observed at 100-mV probing ac voltage, Fig. 2c. The tanδ curves are chosen to give the insight into the behavior of phase angle 'δ' as a function of temperature and voltages. Here, the phase angle gives the information about the voltage lagging with the respect to the applied voltage. The phase angle 'δ' is correlated with permittivity as $\tan\delta = \varepsilon'/\varepsilon''$, where ε' and ε'' are the real and imaginary parts of a complex dielectric permittivity. However, at higher temperature ~ 55 °C, two relaxation peaks have been observed at low probing ac voltages, Fig. 2b, c which is discussed in details in next paragraph. The huge increment in ε', Fig. 2a, clearly indicates towards existence of some other dielectric process in the material because of the fact that in general, the dielectric strength ($\Delta\varepsilon' = \varepsilon_o - \varepsilon_\infty$, where, ε_o and ε_∞ are permittivity at low and high frequencies, respectively) of Goldstone mode and does not change much in SmC* phase with temperature [38].

If one sees carefully in Fig. 2a, the ε' at 20 Hz at 55.5 °C is almost three times more than the ε' at 30 °C in SmC* phase in DHFLC material. This means there must be more than one dielectric process. This is because of the well-known fact that if there are two relaxation process in parallel in sample cell, which indicates the existence of two capacitors working in parallel. Then, the combination of two capacitors gives rise to the additional capacitance resulting into the high permittivity with two relaxation

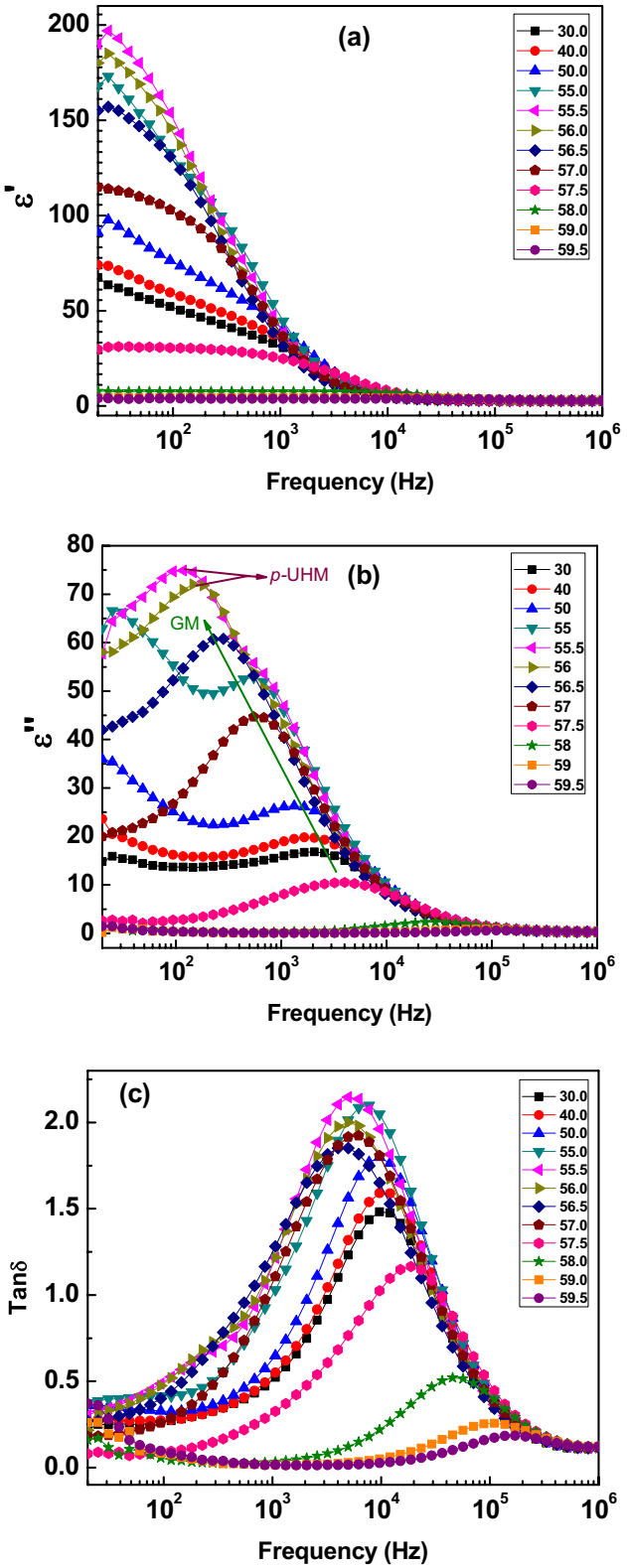

Fig. 2 Permittivity of deformed helix FLC (LAHS-2) at 100-mV probing ac voltage at various temperatures, **a** real part, **b** imaginary parts of complex permittivity and **c** tanδ versus frequency at various temperatures

process. Indeed, there are two dielectric relaxation processes seen when the probing ac voltage is 700 mV in SmC* phase as shown in Fig. 3. One relaxation process at higher frequency is a well-known Goldstone mode; whereas, the relaxation process at lower frequency is due to partially unwound helical mode (p-UHM) of FLC [27]. The saturation of magnitude of p-UHM peak is observed at a particular ac voltage of 700 mV, therefore, in present case, 700 mV peak to peak is considered for the measurement of p-UHM process.

Figure 3 shows the real (ε') and imaginary (ε'') parts of complex dielectric permittivity at probing ac voltage of 700 mV at different temperatures in SmC* phase. As seen in Fig. 3a, the permittivity ε' is maximum at room temperature unlike for 100 mV voltage, and then decreases continuously with the increase in temperature up to the transition temperature (T_c) from SmC* to SmA phase (ferro- to paraelectric) temperature. In ε'' versus frequency curves, Fig. 3b, particularly in tanδ versus frequency curve Fig. 3c, two dielectric processes are clearly seen for lower temperature. One process at higher frequency is due to the Goldstone mode [38] and second process at low frequency is due to p-UHM process as observed by us in DHFLC and conventional FLC materials at room temperature [27]. Such type of mode was also theoretically predicted in FLC as a consequence of phase excitation mode under some constraints of length of sample [9]. It has been experimentally shown that relaxation frequency of such low-frequency process is 2–4 order of magnitude less than Goldstone mode and this order shrinks on increasing probing ac voltage. The relaxation frequency of Goldstone mode process is around 10 kHz in DHFLC material [39] and this new mode p-UHM appears in several hundred Hz in DHFLC material [27]. The Goldstone mode relaxation process in deformed helix FLC material is observed around 10 kHz for thin samples (7–15 µm) and one can expect the p-UHM in the measuring window (above 20 Hz and below Goldstone mode frequency); whereas in FLC, the Goldstone mode process is in several hundred Hz frequency [40] and this mode could be expected in sub-hertz frequency range where the conductivity effect could be quite dominant. However, our recent investigation shows that the p-UHM processes appear even in FLCs [41].

As seen in Fig. 3c, the relaxation frequency of p-UHM in DHFLC process increases with temperature; whereas, the Goldstone mode relaxation frequency first remains constant and then decreases near T_c. It has been observed that both the modes merge near T_c. If we see ε'' versus frequency curves, the Goldstone mode relaxation frequency continuously decreases with temperature which is due to the fact that ε'' is obtained by multiplying tanδ with ε' and ε' is itself also quite high in SmC* phase; therefore, the p-UHM is not clearly reflected as seen in Fig. 3b. In further studies, tanδ

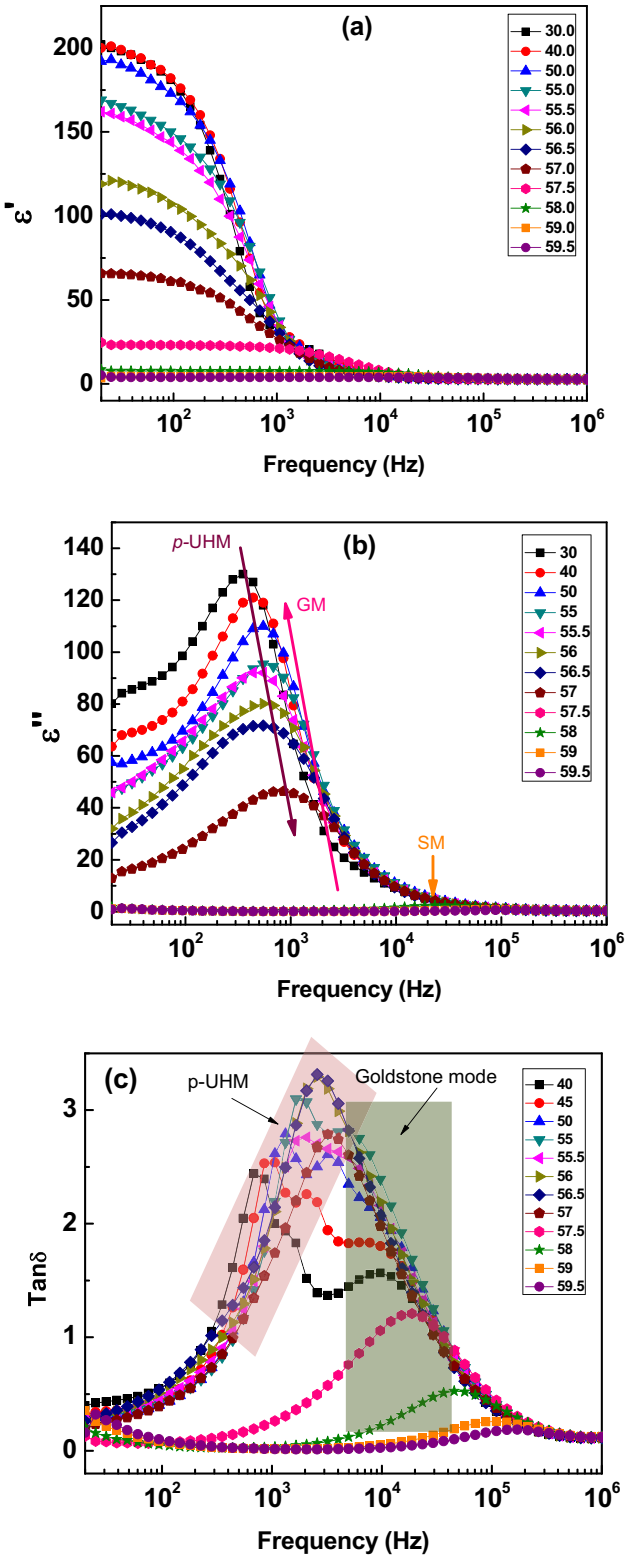

Fig. 3 Permittivity at 700-mV probing ac voltage at various temperatures, **a** real part, **b** imaginary parts of complex permittivity and **c** tanδ versus frequency at various temperatures

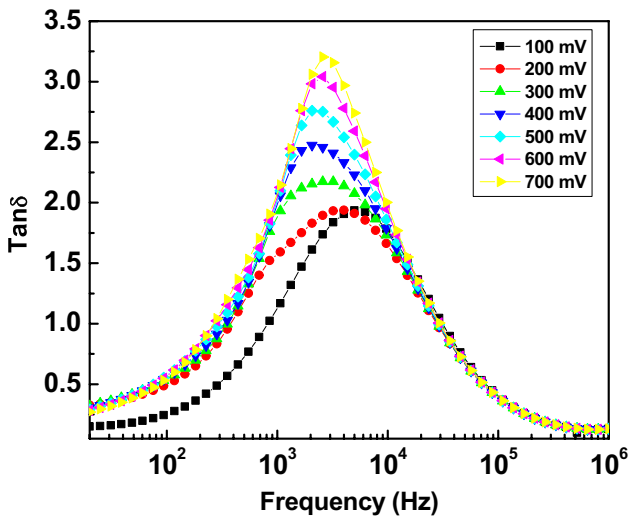

Fig. 4 Tanδ as a function of frequency at various probing ac voltages at 56.5 °C

versus frequency plots are taken into consideration for the estimation of relaxation process.

Figure 4 shows tanδ as a function of frequency at different probing ac voltage close to T_c at 55.5 °C temperature. As seen in the figure, a single peak appears (Goldstone mode) at 100-mV measuring field and as the field is increased to 200 mV, a hump starts appearing related to *p*-UHM. Again as the field is increased further, this hump starts shifting towards the Goldstone mode relaxation process and merges with Goldstone mode at 700 mV measuring field. This means that *p*-UHM process appears even for lower measuring field depending upon the favorable condition of the unwound of helical structure at the interface of substrate and bulk in DHFLC material.

3.3 Effect of temperature on Goldstone mode and *p*-UHM

Figure 5 shows the dielectric strength, $\Delta\varepsilon$ with temperature at different probing ac voltages which are found to increase first and then decrease with temperature for lower probing voltage. As the amplitude of ac voltage is increased, $\Delta\varepsilon$ becomes constant and then decreases around T_c temperature in DHFLCs. As seen in figure, the $\Delta\varepsilon$ is maximum at 500 mV from 30 to 40 °C temperature; whereas at higher temperature (50 °C), the $\Delta\varepsilon$ is maximum at 300 mV. With further increase in temperature, the $\Delta\varepsilon$ is maximum at 200 mV. This decreasing trend of probing voltage with temperature for maximum $\Delta\varepsilon$, suggests that there is a definite threshold probing voltage for *p*-UHM process, beyond which the $\Delta\varepsilon$ would decrease. This means that unwound helical fluctuation causing high permittivity (dielectric strength) is maximum at a particular threshold probing ac field and

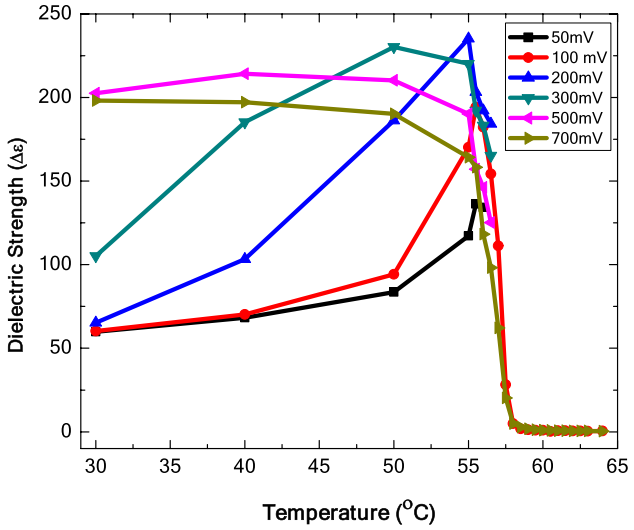

Fig. 5 Dielectric strength ($\Delta\varepsilon$) of p-UHM as a function of temperature at various amplitude of probing ac voltage

this probing ac field decreases with temperature for p-UHM process (Fig. 5).

Figure 6 is about the relaxation frequency of Goldstone mode and p-UHM process as a function of temperature at different probing ac voltages in SmC* phase. As shown in the inset of Fig. 6a, the relaxation frequency of Goldstone mode process for lower probing voltage decreases up to 55 °C and then increases with the temperature. However, for higher measuring voltages 500 and 700 mV, the relaxation frequency remains almost constant upto 56 °C and then decreases with the increase in temperature in SmC* phase as seen in Fig. 6a. This means for lower measuring voltage, the Goldstone mode is coupled with the p-UHM, resulting in decrease in relaxation frequency as also reflected in Fig. 4. The polarization of individual layer of bulk helix is oriented in all possible directions to complete the helical structure, i.e., zero polarization; whereas, the polarization of partially unwound helical structure near the surfaces of substrates has some net polarization due to the larger number of dipoles oriented in one direction because of high surface anchoring effect. When two frequencies approach each other, the resultant of dipole moments of phason fluctuations/Goldstone mode and the surface dipoles produces the net dipole moment resulting into a new relaxation process. As shown in Fig. 6b, the relaxation frequency of p-UHM increases continuously with temperature for lower and higher measuring fields; whereas, the Goldstone mode relaxation frequency decreases at lower ac field with the increase in temperature up to the T_c in SmC* phase. At higher amplitude of applied probing field, the relaxation frequency of Goldstone mode decreases close to T_c only. However, for measuring field 100 mV, the p-UHM is observed at higher temperatures (above 50 °C)

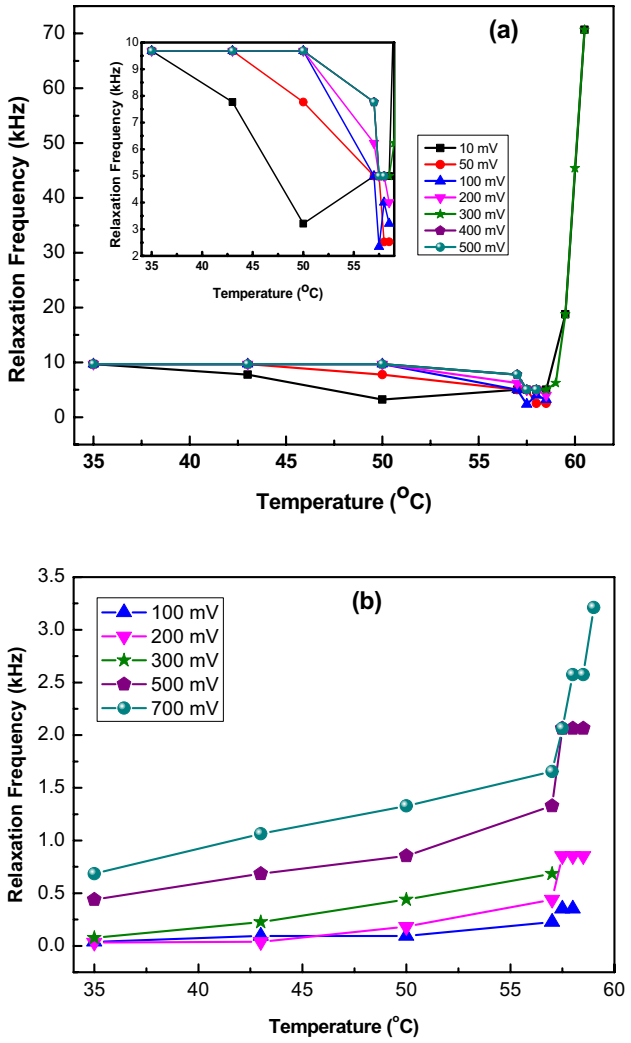

Fig. 6 **a** Relaxation frequency (estimated from tanδ curve) (ν_R) of Goldstone mode of deformed helix FLC as a function of temperature at various probing ac voltage. Inset shows the enlarge view of relaxation frequency from 35° to 55 °C, **b** Relaxation frequency of p-UHM (ν_R) as a function of temperature at various probing ac voltages

in SmC* phase, as seen in Figs. 2b and 6b. The probing ac voltage-dependent measurement at 56.5 °C, Fig. 3, shows the appearance of p-UHM at 200 mV and above fields. The p-UHM merges with Goldstone mode above 400 mV. The relaxation frequency of p-UHM process increases with temperature for higher measuring voltage, Fig. 6b.

Figure 7 shows the difference in the relaxation frequency ($\Delta\nu$) of Goldstone and p-UHM mode ($\Delta\nu = \nu_{GM} - \nu_{p-UHM}$) with temperature. As seen in the figure, the difference is larger for lower measuring voltages because of the fact that the relaxation frequencies of the Goldstone mode and p-UHM process are well separated and this difference decreases with temperature.

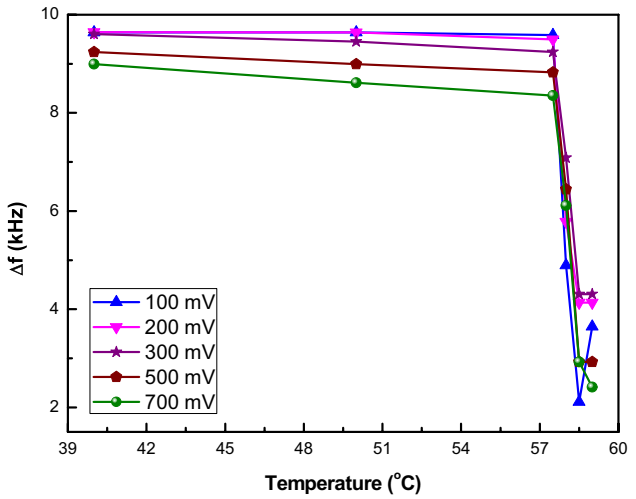

Fig. 7 Difference in relaxation frequencies (ν_R) of Goldstone mode and *p*-UHM as a function of temperature at various probing ac voltage

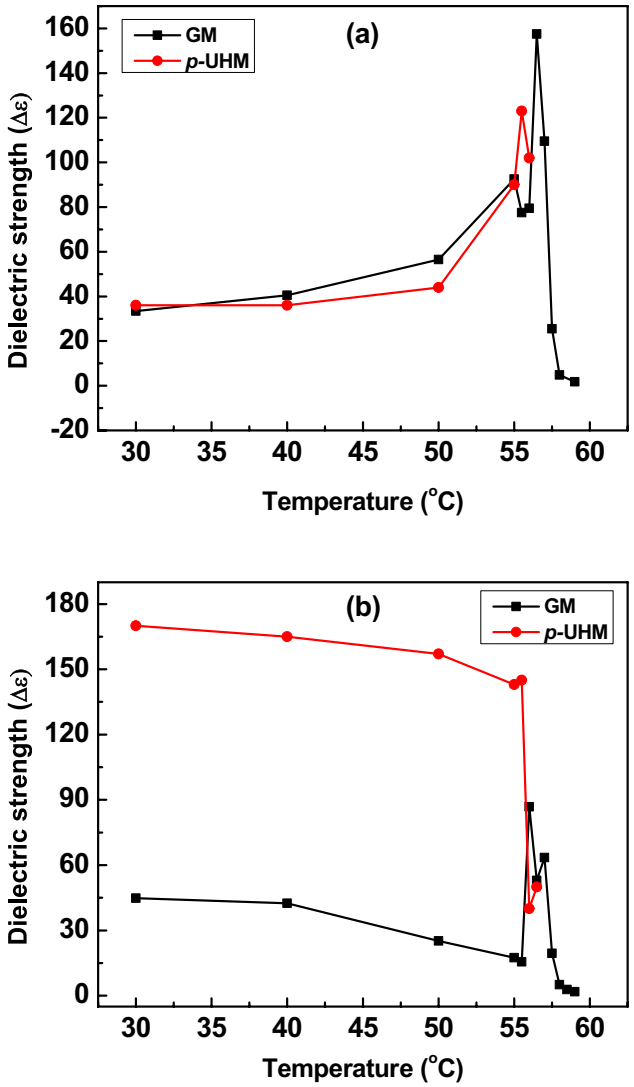

Fig. 8 Dielectric strength ($\Delta\varepsilon$) of *p*-UHM and Goldstone mode with temperature at **a** 100-mV and **b** 700-mV oscillating field, calculated theoretically in SmC* phase

The separation of the two processes in the ε' is difficult; therefore, the dielectric strength is calculated by fitting the experimental data using Cole–Cole model, Eqs. (1)–(4). However, the behavior of dielectric strength of Goldstone mode and *p*-UHM process is different as shown in Fig. 8, which is calculated using the above equations theoretically. Other parameters like distribution parameter (α), relaxation time (τ), relaxation frequencies by ε'' and tanδ curves with temperature were calculated and compared with the experimental results and shown in the tables for the data at low (100 mV) and high (700 mV) oscillating voltages for *p*-UHM, Goldstone, and soft modes (Tables 1, 2, 3, 4). As seen in the figure, the behavior of the dielectric strength with temperature at low oscillating voltage (100 mV) is almost the same and increases close to the T_c temperature. Figure 8a; whereas, the dielectric strength at higher oscillating voltage (700 mV), the dielectric strengths of *p*-UHM and Goldstone mode are well separated as seen in Fig. 8b. This means that the contribution of *p*-UHM is very large as compared with the Goldstone mode at higher ac voltage. At low voltage, both the modes are independent of temperature in which the intrinsic behavior of Goldstone mode is observed with temperature in SmC* phase. This could be the reason that there are always anomalies in the literature for the behavior of Goldstone mode with the increase in temperature in SmC* phase of FLC materials. From the experimental and theoretical observations, it is clear that the *p*-UHM process hinders the real behavior of Goldstone mode with temperature in middle thickness range (~ 10 μm) of FLC cells.

The dielectric processes is analyzed by studying the relaxation time distribution parameter (α) which shows symmetric behavior of the relaxation process and is expected to bring up the interaction of two dielectric processes (GM and *p*-UHM). The process is expected to be more ordered and tends to approach towards the ideal Debye model if the value of α tends to be negligible. Similarly, larger value of α will extend the distribution of relaxation time resulting in the interference of two processes with each other. If α approaches zero, the molecules will have higher symmetry of ordered dipolar process and when α approaches 1, the symmetry of the molecules in FLC system will be less due to the interference of more than one processes. The Cole–Cole dielectric model is used to fit the dielectric data of Figs. 2 and 3. The data used in fitting process are given the Tables 1, 2, 3 and 4. The α distribution parameter plotted in Fig. 9a is obtained from the Tables 1 and 2. The behavior of both the modes (*p*-UHM and GM) is same at low voltage (100 mV). However, a slight increment near *Tc* suggests the merging

Table 1 Experimental ε′ as a function of frequency (Fig. 2a) fitted using Cole–Cole model for various thicknesses at 100 mV for GM process and soft mode

Sample	Temperature (°C)	100 mV							
		Goldstone mode and Soft mode							
		ε_∞	ε_o	Dielectric strength, ($\Delta\varepsilon$)	α	Relaxation time, τ (fitting) $\times 10^{-3s}$	Relaxation frequency, ε'' (fitting), Hz	Relaxation frequency, tanδ (fitting), Hz	Relaxation frequency, tanδ (experimental), Hz
LAHS-2	**30**	2.6	36	33.4	0.07	0.06	2653.9	9875.3	9686
	40	2.5	43	40.5	0.08	0.068	2341.7	9711.7	9686
	50	2.5	59	56.5	0.09	0.065	2449.7	11,900.9	9686
	55	2.5	95	92.5	0.06	0.165	965	5949	7767
	55.5	2.5	80	77.5	0.02	0.16	995.2	5629.8	4994
	56	2.5	82	79.5	0.06	0.18	884.6	5066.4	4994
	56.5	2.5	160	157.5	0.185	0.505	315.3	2522.5	4994
	57	2.5	112	109.5	0.15	0.27	589.7	3947.4	4994
	57.5	2.5	28	25.5	0.14	0.05	3184.7	10,658	18,786
	58	2.7	7.55	4.85	0.03	0.0000058	27,454.426	45,909.65	45,439
	59	2.7	4.46	1.76	0.01	0.000002	79,617.834	102,328.3	109,907

ε_∞ permittivity at high frequencies; ε_o permittivity at low frequencies

Table 2 Experimental ε′ as a function of frequency (Fig. 2a) fitted using Cole–Cole model for various thicknesses at 100 mV for *p*-UHM process

Sample	Temperature	100 mV							
		p-UHM							
		ε_∞	ε_o	Dielectric strength, ($\Delta\varepsilon$)	α	Relaxation time, τ (fitting) $\times 10^{-3s}$	Relaxation frequency, ε'' (fitting), Hz	Relaxation frequency, tanδ (fitting), Hz	Relaxation frequency, tanδ (experimental), Hz
LAHS-2	**30**	34	70	36	0.25	1.6	300.4	798.9	684
	40	39	75	36	0.2	1.3	346.1	827.4	1064
	50	56	100	44	0.15	1.9	419	1077.1	1327
	55	90	180	90	0.1	1.8	497.6	1615	1655
	55.5	77	200	123	0.06	1.25	454.9	1586	2064
	56	78	180	102	0.01	1.2	144.7	177.2	2574
	56.5	34	70	36	0.25	1.6	206.7	292.4	2574

ε_∞permittivity at high frequencies; ε_o permittivity at low frequencies

of two processes. Figure 9b shows the behavior of distribution parameter for DHFLC material at 700-mV measuring ac voltages for various temperatures. It is seen that the behavior of α for GM with respect to temperature decreases and is minimum ~ 50 °C, and then again slightly increases near transition temperature, which is expected as Goldstone mode merges with soft mode. Again for *p*-UHM process, the α parameter is observed to increase with temperature and tends to merge with Goldstone mode near the transition temperature. It is worth mentioning here that *p*-UHM is contributing in collective dielectric process and suggests that the helix becomes more soft or flexible at higher temperatures close to T_c. The *p*-UHM process is seen at lower temperatures but merges with the Goldstone mode at higher temperature near T_c, resulting in the broad peak.

3.4 Effect of dc bias field on Goldstone mode

As discussed above, it is difficult to find out the independent behavior of Goldstone mode well below T_c in SmC* phase because of the fact that for lower temperature, *p*-UHM interferes and at higher temperature, soft mode hinders the Goldstone mode process [41]. One can find out the behavior of Goldstone mode independent of *p*-UHM process well below T_c in SmC* by suppressing the unwound helical structure by applying a high dc

Table 3 Experimental ε' as a function of frequency (Fig. 3a) fitted using Cole–Cole model for various thicknesses at 700 mV for Goldstone mode and soft mode

Sample	Temperature	700 mV							
		Goldstone mode and soft mode							
		ε_∞	ε_o	Dielectric strength, ($\Delta\varepsilon$)	α	Relaxation time, τ (fitting) $\times 10^{-3s}$	Relaxation frequency, ε'' (fitting), Hz	Relaxation frequency, tanδ (fitting), Hz	Relaxation frequency, tanδ (experimental), Hz
LAHS-2	**30**	2.2	47	44.8	0.2	0.11	1447.5	6690.9	9686
	40	2.5	45	42.5	0.1	0.1	1592.3	6755.7	6228
	50	2.8	28	25.2	0.01	0.065	2449.7	7746.8	7767
	55	2.5	20	17.5	0.05	0.05	3184.7	9007.7	4994
	55.5	2.5	18	15.5	0.08	0.05	3184.7	8545.4	4994
	56	3.2	90	86.8	0.01	0.205	776.7	4119.3	2574
	56.5	3	56	53	0.025	0.15	1061.5	4586.5	2574
	57	2.5	66	63.5	0.17	0.23	692.3	3557.2	3211
	57.5	2.5	22	19.5	0.085	0.029	5490.8	16,288.6	18,786
	58	2.5	7.6	5.1	0.03	0.0056	28,434.9	49,578	45,439
	58.5	2.7	5.5	2.8	0.02	0.0032	49,761.1	71,021.5	70,669
	59	2.7	4.46	1.78	0.01	0.000002	79,617.8	102,328.3	109,907

ε_∞ permittivity at high frequencies; ε_o permittivity at low frequencies

Table 4 Experimental ε' as a function of frequency (Fig. 3a) fitted using Cole–Cole model for various thicknesses at 700 mV for p-UHM process

Sample	Temperature	700 mV							
		p-UHM							
		ε_∞	ε_o	Dielectric strength, ($\Delta\varepsilon$)	α	Relaxation time, τ (fitting) $\times 10^{-3s}$	Relaxation frequency, ε'' (fitting), Hz	Relaxation frequency, tanδ (fitting), Hz	Relaxation frequency, tanδ (experimental), Hz
LAHS-2	**30**	28	198	170	0.009	0.53	300.4	798.9	684
	40	35	200	165	0.05	0.46	346.1	827.4	1064
	50	28	185	157	0.06	0.38	419	1077.1	1327
	55	15	158	143	0.09	0.32	497.6	1615	1655
	55.5	13	158	145	0.13	0.35	454.9	1586	2064
	56	80	120	40	0.05	1.1	144.7	177.2	2574
	56.5	50	100	50	0.05	0.77	206.7	292.4	2574

ε_∞permittivity at high frequencies; ε_o permittivity at low frequencies

bias field in SmC* phase [42]. Figure 10 shows the real and imaginary parts of complex permittivity with different temperatures in SmC* phase at the bias field of 10 V, which is sufficient to suppress the helical structure almost completely. As seen in Fig. 10a, the permittivity is suppressed and decreased continuously with temperature up to the few degrees below the T_c. The ε'' and tanδ Fig. 10b, c show that the relaxation frequency of the Goldstone mode increases continuously with temperature up to the T_c. It is worth to point out here that the ε'' and tanδ curves are in the same sequence because of the fact that the permittivity is low due to the suppression of Goldstone mode in SmC* phase. As seen in Fig. 10d, the dielectric strength ($\Delta\varepsilon$) or the permittivity (ε) decreases continuously in deep SmC* phase and then increases near T_c temperature at such a high bias field of 10 Volts. The contribution (Δ') is maximum at T_c because of the contribution of soft mode and not because of *p*-UHM, and then again starts decreasing in SmA phase [17].

Figure 11 shows the relaxation frequency of Goldstone mode and soft mode with temperature at a bias of 10 Volts. As seen in figure, the relaxation frequency of Goldstone mode is almost constant or slightly increases with temperature. The soft mode frequency behaves perfectly like

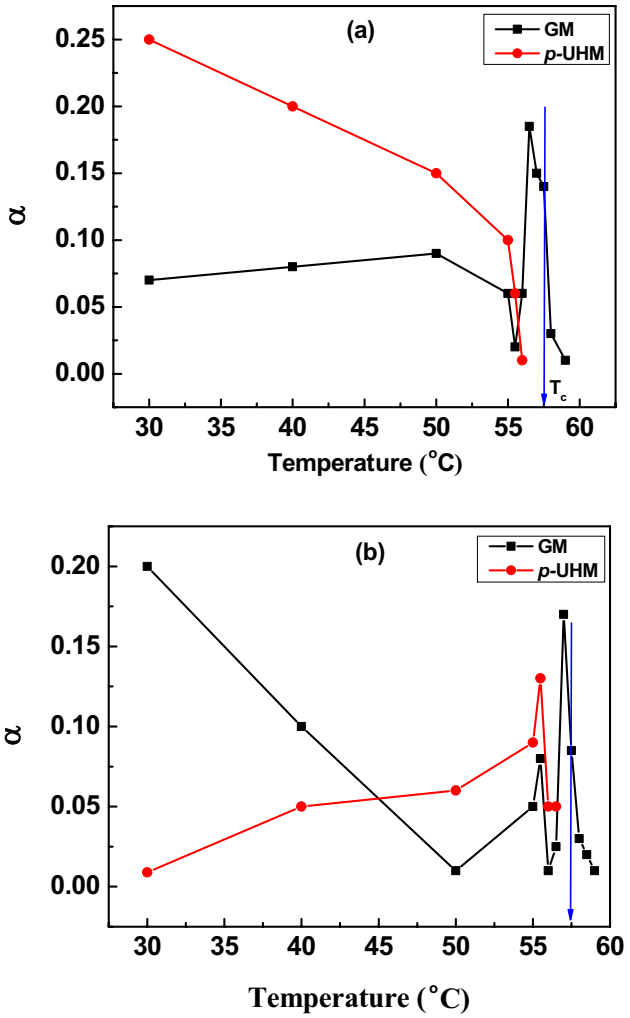

Fig. 9 Distribution parameter for *p*-UHM and GM of DHFLC as a function of temperature at **a** 100 mV and **b** 700 mV

"V" shape at the T_c temperature in SmC* and SmA* phases where Goldstone mode is isolated in SmC* phase by applying a high dc bias field [17].

4 Activation energy

Since the *p*-UHM is dependent on temperature, the activation energy is supposed to give information about the process. It represents the well-known Arrhenius-type behavior which is used to know the activation energy by the equation [38]:

$$\nu_r = \nu_o e^{-E_a/k_B T}, \tag{7}$$

where ν_r represents the relaxation frequency and ν_o is the relaxation frequency at high temperature. E_a is the activation energy connected with the orientating potential barrier of liquid crystal phase. "*T*" is the temperature of the sample in the unit of Kelvin and k_B the Boltzmann's constant. Generally, the phase of liquid crystals is characterized by its intrinsic activation energy [43–45]. It has been observed Fig. 12 that the Arrhenius plot of *p*-UHM is almost linear in the SmC* phase for the sample under study implying that the activation of the *p*-UHM process remains same throughout the phase. The values of activation energy for various probing ac voltages are shown in Fig. 12.

5 UV–visible measurements

The electro-optical textures of FLCs have confirmed the variation in the transmission [27]. Therefore, the measurement of optical transmission in the UV–visible range at room temperature is performed for the analysis of the wavelength-dependent transmission at various probing voltage. The unpolarized light is made plane polarized by placing the polarizer after the source and before the sample cell. The analyzer is fixed between the detector and sample cell. The optic axis of polarizer and analyzer is fixed at 90° angle to each other. The DHFLC sample is placed in between them with the rubbing direction of sample cell at 45° to both the polarizer and analyzer. The transmission of the DHFLC cell has been recorded at various amplitudes of applied ac voltages. As can be seen in Fig. 13a, the blue shifts of 6.8- and 9.3-nm wavelengths are observed for the peaks 573.8 and 642 nm, respectively, at amplitudes of 0 V and 8 V at 100-Hz frequency using arbitrary wave form generator. However, there is no observable peak shift at any wavelength up to 1 V because of the fact that the molecular reorientation does not take place up to 1 V but the partial helical unwinding takes place. In the dielectric spectra also, the *p*-UHM peak is quite dominating at these voltages. Combining the two observations of dielectric and optical, it can be said that the process of *p*-UHM is not due to molecular reorientation because a molecular reorientation would cause the change in the transmission wavelength of the sample. Hence, no peak shift should be observed up to 1 V and is true as observed in Fig. 13a. This means that *p*-UHM process is due to partial unwound of helical fluctuations as observed in dielectric spectroscopy. The relaxation Fig. 4c at lower frequency suggests that this mode is due to unwound helical fluctuations. On further increase in the amplitude of applied voltage, the observed blue shift in optical spectra is attributed to molecular reorientation process resulting in the increase in the transmission and shift in the optical peaks in UV–visible spectra. The intensity increases linearly with the increase in the probing ac voltage. On the contrary, Fig. 13b reveals that at a constant frequency of 100 kHz, there is almost no remarkable change in the intensity of optical spectra at any

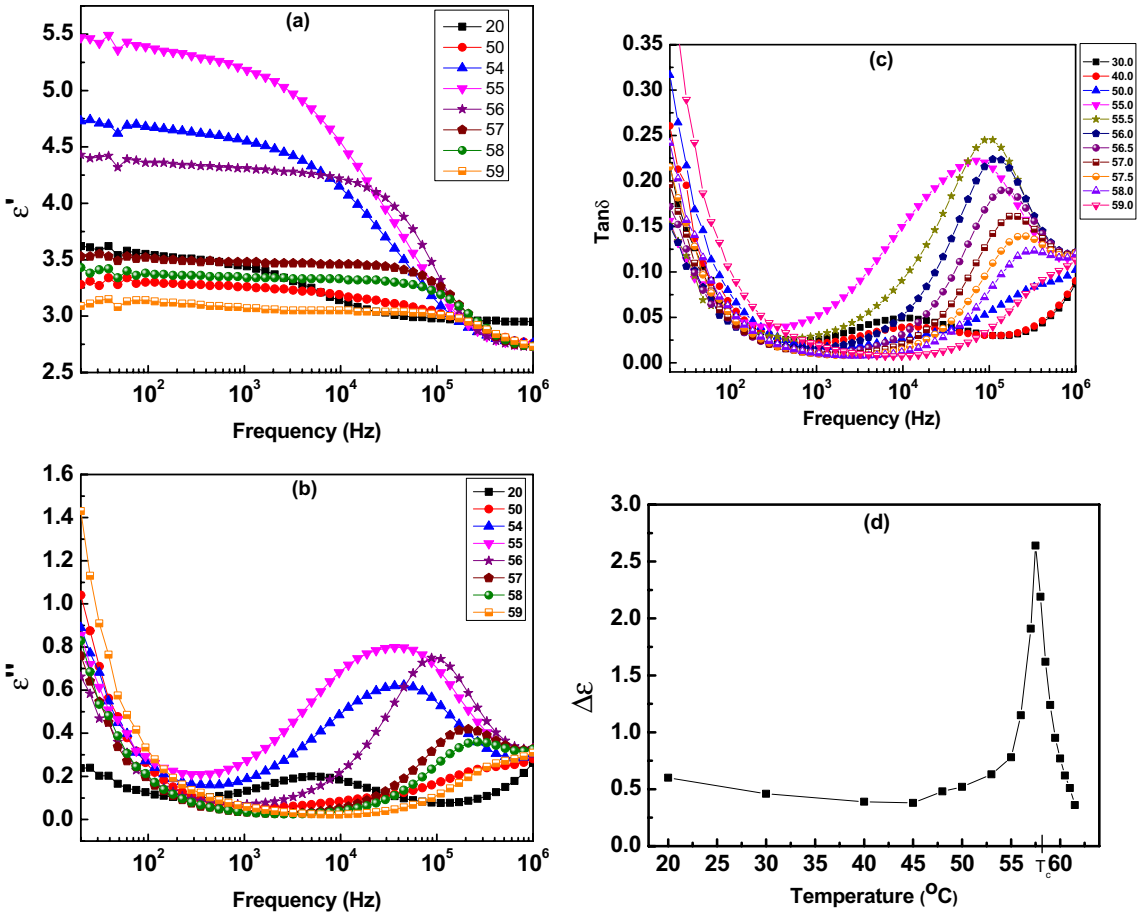

Fig. 10 Dielectric spectra of deformed helix FLC at 10-V bias and at 700-mV probing ac voltage **a** real part, **b** imaginary part of complex permittivity, **c** tanδ vs frequency, and **d** dielectric strength at various temperatures

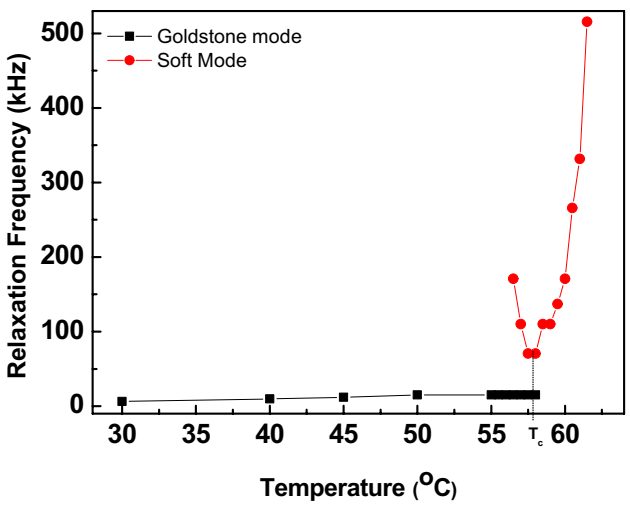

Fig. 11 Relaxation frequency of Goldstone mode and soft mode of deformed helix FLC as a function of temperature, at a bias of 10 V

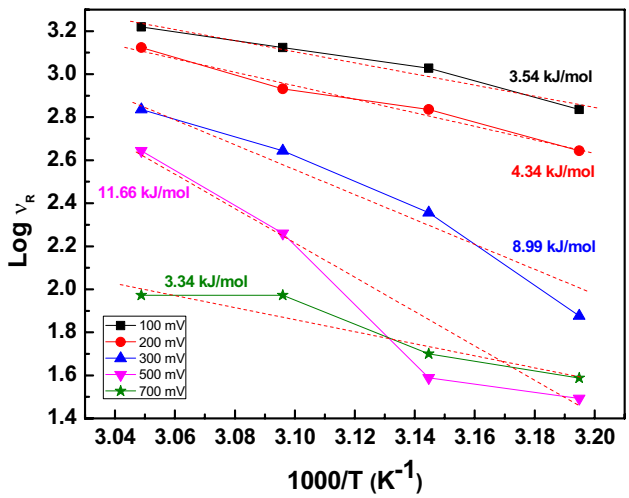

Fig. 12 Activation energy of *p*-UHM of deformed helix FLC at various probing ac voltages

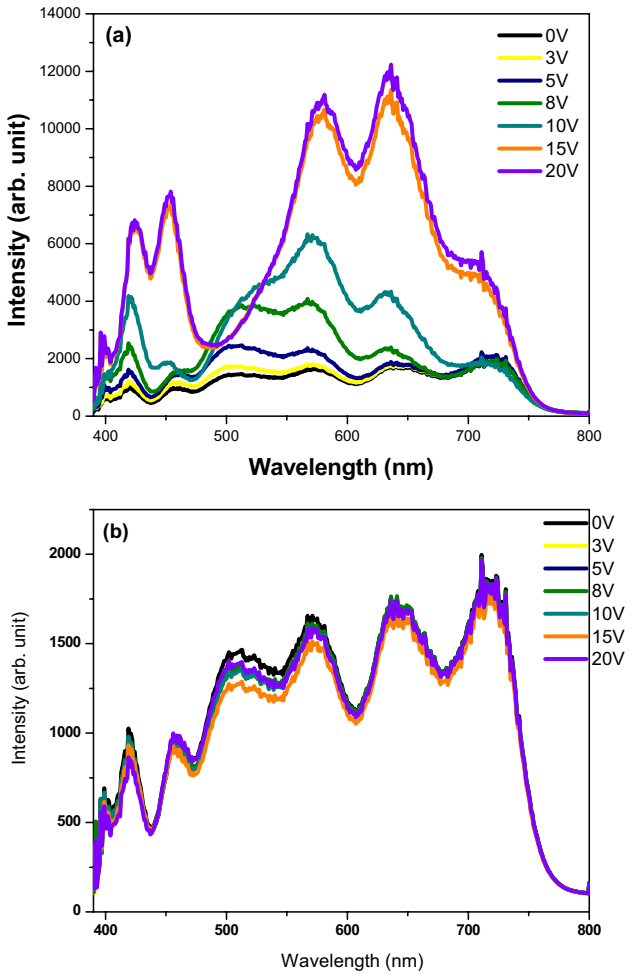

Fig. 13 UV–visible measurement of deformed helix FLC (LAHS-2) at **a** 100 Hz, **b** 100 kHz of various strengths of applied probing ac voltage

wavelength. One can say that the dielectric property at such a high frequency (100 kHz) is not due to phase (Goldstone mode) or tilt angle (soft mode) fluctuations.

6 Conclusions

The DHFLC has been studied under the strongly rubbed surfaces at different temperatures in SmC* phase. It is found that a low relaxation process, called *p*-UHM (partially unwound helical mode), has been observed at high amplitude of probing ac voltage at a lower frequency than the Goldstone mode process in SmC* phase. The high anchoring has modulated the helical structure at the interface of substrate and FLC which originates the *p*-UHM process. On the other hand, the bulk helical structure is responsible for the Goldstone mode process. The high enough amplitude of probing ac voltage is required to realize the *p*-UHM due to the fact that the FLC molecules are strongly bound to the substrate. The Goldstone mode relaxation frequency is found to decrease with temperature near T_c. However, the relaxation frequency of *p*-UHM is found to increase throughout the SmC* phase. The *p*-UHM process is found to hinder the general behavior of Goldstone mode in SmC* phase. To know the independent behavior of Goldstone mode, one needs to apply the high dc bias to suppress the helical structure of the FLC material. The new relaxation process is highly dependent on the probing ac voltage and dc bias voltage; therefore, it is anticipated that the mode could be utilized for low-power FLC-based electro-optical devices. The applicability of *p*-UHM in devices is due to the interfacial phenomenon where the electric field strength is more than in the bulk, and the helix of FLC is unwound that resulted in the induction of net spontaneous polarization near the surface. The higher electric field would apply a torque on the induced and spontaneous polarization that resulted into a low field switching [27].

Acknowledgements We sincerely thank the Director, Dr. D. K. Aswal, National Physical Laboratory, New Delhi for his continuous encouragement in this work. We would like to thank the Department of Science and Technology, New Delhi, India for financial support through Project Science and Engineering Research Board Grant GAP-150632 at NPL, New Delhi, India. We (A.M.B. and A.B.) are thankful to Council of Scientific and Industrial Research (CSIR, India) (21/(0986)/13-EMR-II) for the financial assistance under an Emeritus Scheme.

References

1. L.A. Beresnev, V.G. Chingrinov, D.I. Dergachev, E.P. Poshidaev, J. Funfschilling, M. Schadt, Deformed helix ferroelectric liquid crystal display: a new electrooptic mode in ferroelectric chiral smectic C liquid crystals. Liq. Cryst. **5**, 1171–1177 (1989)
2. F.L. Vladimirov, A.N. Chaika, N. Collings, Spatial light modulator based on hydrogenated amorphous silcon/deformed-helix ferroelectric liquid crystal structure: influence of dielectric mirror. Ferroelectrics **246**, 1175 (2000)
3. A.D. Kiselev, E.P. Pozhidaev, V.G. Chigrinov, H.S. Kwok, Polarization-grating approach to deformed helix ferroelectric liquid crystals with subwavelength pitch. Phys. Rev. E **83**(3), 031703 (2011)
4. J. Prakash, A. Choudhary, D.S. Mehta, A.M. Biradar, Effect of surface anchoring on optical bistability in deformed helix ferroelectric liquid crystals. Mol. Cryst. Liq. Cryst. **511**, 1881658 (2009)
5. S. Kaur, A.K. Thakur, R. Chauhan, S.S. Bawa, A.M. Biradar, Bistability in deformed helix ferroelectric liquid crystal. J. Appl. Phys. **96**, 2547 (2004)
6. A. Lapanik, A. Rudzki, B. Kinkead, H. Qi, T. Hegmann, W. Haase, Electrooptical and dielectric properties of alkylthiol-capped gold nanoparticle–ferroelectric liquid crystal nanocomposites: influence of chain length and tethered liquid crystal functional groups. Soft Matter **8**, 8722 (2012)
7. A. Choudhary, G. Singh, A.M. Biradar, Advances in gold nanoparticle–liquid crystal composites. Nanoscale **6**, 7743 (2014)

8. N. Sood, S. Khosla, D. Singh, S.S. Bawa, Dielectric investigation of pure carbon nanotube-doped deformed helix ferroelectric liquid crystals. Liq. Cryst. **39**(10), 1169 (2012)
9. B.K. Urbanc, B. Zeks, Phase-excitation spectrum of ferroelectric liquid crystals in an external static electric field. Phys. Rev. E **52**(4), 3892 (1995)
10. J.K. Song, U. Manna, J.K. Vij, Mechanism of field-induced unwinding of SmC* helix and bias field dependencies of dielectric permittivity and effective polarization. Euro Phys. Lett. **82**, 26003 (2008)
11. L.A. Beresnev, M. Pfeiffer, S.A. Pikin, W. Haase, L.A. Blinov, Domain mode—a novel relaxation process in ferroelectric liquid crystals. Ferroelectrics **132**, 99 (1992)
12. R.B. Meyer, Ferroelectric liquid crystals; a review. Mol. Cryst. Liq. Cryst. **40**, 33 (1977)
13. R.B. Meyer, Effects of electric and magnetic fields on the structure of cholesteric liquid crystals. Appl. Phys. Lett. **12**, 281 (1968)
14. A.D. Rey, Flow alignment in the helix uncoiling of sheared cholesteric liquid crystals. Phys. Rev. E **53**, 4198 (1996)
15. S.I. Suwa, H. Hoshi, Y. Takanishi, K. Ishikawa, H. Takezoe, B. Zeks, Helix unwinding process in a short-pitch ferroelectric liquid crystal mixture studied by conoscopy. Jpn. J. Appl. Phys. **42**, 1335 (2003)
16. S.S. Bawa, A.M. Biradar, S. Chandra, Dynamics of helix winding, unwinding and switching of ferroelectric liquid crystals. Jpn. J. Appl. Phys. **26**(1), 189 (1987)
17. E. Pozhidaev, V. Chigrinov, A. Murauski, V. Molkin, D. Tao, H.S. Kwok, V-shaped electro-optical mode based on deformed-helix ferroelectric liquid crystal with subwavelength pitch. J. SID **20**(5), 273 (2012)
18. S. Uto, A helix unwinding process in ferroelectric liquid crystals with fixed boundaries. J. Appl. Phys. **97**(1), 014107 (2005)
19. A.V. Kaznacheev, E.P. Pozhidaev, Effect of boundary surfaces on the effective dielectric susceptibility of the helical structure of a ferroelectric liquid crystal. J. Exp. Theor. Phys. **121**, 355–361 (2015)
20. V.V. Kesaev, A.D. Kiselev, E.P. Pozhidaev, Modulation of unpolarized light in planar-aligned subwavelength-pitch deformed-helix ferroelectric liquid crystals. Phys. Rev. E **95**, 032705 (2017)
21. S.P. Kotova, S.A. Samagin, E.P. Pozhidaev, A.D. Kiselev, Light modulation in planar aligned short-pitch deformed-helix ferroelectric liquid crystals. Phys. Rev. E **9**, 062502 (2015)
22. Z. Brodzeli, L. Silvestri, A. Michie, Q. Guo, E.P. Pozhidaev, V. Chigrinov, F. Ladouceur, Reflective mode of deformed-helix ferroelectric liquid crystal cells for sensing applications. Liq. Cryst. **40**(10), 1427 (2013)
23. A. Mukherjee, M. Rahman, S.S. Bhattacharyya, A. Yoshizawa, B.K. Chaudhuri, Dielectric permittivity-voltage hysteresis in deformed helix ferroelectric liquid crystal. Chem. Phys. Lett. **457**, 315 (2008)
24. A. Bubnov, C. Vacek, M. Czerwiński, T. Vojtylová, W. Piecek, V. Hamplová, Design of polar self-assembling lactic acid derivatives possessing submicrometre helical pitch. Beilstein J. Nanotechnol. **9**, 333 (2018)
25. L. Silvestri, H. Srinivas, F. Ladoveeur, Effective dielectric tensor of deformed helix ferroelectric liquid crystals with subwavelength pitch and large tilt angle. Phys. Rev. E **98**(5), 052707 (2018)
26. J. Fitas, M. Marzec, K. Kurp, M. Żurowska, M. Tykarska, A. Bubnov, Electro-optic and dielectric properties of new binary ferroelectric and antiferroelectric liquid crystalline mixtures. Liq. Cryst. **44**(9), 1468 (2017)
27. A. Choudhary, A. Bawa, Rajesh, S.P. Singh, A.M. Biradar, Dielectric relaxation process of a partially unwound helical structure in ferroelectric liquid crystals. Phys. Rev. E **95**, 062702 (2017)
28. A. Bawa, L.K. Gangwar, A. Dhingra, A. Choudhary, Rajesh, S.P. Singh, W. Haase, A.M. Biradar, Polarisation-dependent dielectric processes in ferroelectric liquid crystals. Liq. Cryst. **46**(2), 166 (2018)
29. J.M. Geary, J.W. Goodby, A.R. Kmetz, J.S. Patel, The mechanism of polymer alignment of liquid crystal materials. J. Appl. Phys. **62**(10), 4100 (1987)
30. S. Ishihara, H. Wakemoto, K. Nakazima, Y. Matsuo, The effect of rubbed polymer films on liquid crystal alignment. Liq. Cryst. **4**(6), 669 (1989)
31. W. Zheng, C.H. Lu, Y.C. Ye, Effects of mechanical rubbing on surface tension of polyimide thin films. Jpn. J. Appl. Phys. **47**, 1651 (2008)
32. E.P. Haridas, A.M. Biradar, G.K. Chadha, Effect of surface anchoring on electro-optical characteristics of high tilt angle FLC materials. Ferroelectrics **211**(1), 9 (1998)
33. F.V. Podgornov, A.M. Suvorova, A.V. Lapanik, W. Haase, Electrooptic and dielectric properties of ferroelectric liquid crystal/single walled carbon nanotubes dispersions confined in thin cells. Chem. Phys. Lett. **479**, 206 (2009)
34. K.S. Cole, R.H. Cole, Dispersion and absorption in dielectrics I. Alternating current characteristics. J. Chem. Phys. **9**, 341 (1941)
35. W. Haase, S. Wróbel (eds.), *Relaxation phenomena: liquid crystals, magnetic systems, polymers, high-Tc superconductors, metallic glasses* (Springer, Berlin, 2003)
36. A. Levstik, T. Carlsson, C. Filipic, I. Levstik, B. Zeks, Goldstone mode and soft mode at the smectic—a smectic-C* phase transition studied by dielectric relaxation. Phys. Rev. A **35**, 3527 (1987)
37. T. Carlsson, B. Žekš, C. Filipič, A. Levstik, Theoretical model of the frequency and temperature dependence of the complex dielectric constant of ferroelectric liquid crystals near the smectic-C*-smectic—a phase transition. Phys. Rev. A **42**, 877 (1990)
38. A.M. Biradar, S. Wrobel, W. Haase, Dielectric relaxation in the smectic-A* and smectic-C* phases of ferroelectric liquid crystal. Phys. Rev. A **39**, 2693 (1989)
39. A. Kumar, J. Prakash, A. Choudhary, A.M. Biradar, Dielectric and electro-optical studies of glycerol/ferroelectric liquid crystal mixture at room temperature. J. Appl. Phys. **105**, 124101 (2009)
40. T. Joshi, A. Kumar, J. Prakash, A.M. Biradar, Low frequency dielectric relaxations of gold nanoparticles/ferroelectric liquid crystal composites. Liq. Cryst. **37**(11), 1433 (2010)
41. L.K. Gangwar, A. Bawa, A. Choudhary, S.P. Singh, Rajesh, A.M. Biradar, Collective dielectric processes at the transition temperature of the Sm-C* and Sm-A* phase in a ferroelectric liquid crystal. Phys. Rev. E **97**, 062707 (2018)
42. A.M. Biradar, S.S. Bawa, W. Haase, Goldstone mode behaviour in deformed helix ferroelectric liquid crystal materials. Ferroelectrics **256**, 201 (2001)
43. P.G. de Gennes, Calcul de la distorsion d'une structure cholesterique par un champ magnetique. Solid State Commun. **6**(3), 163 (1968)
44. Z.H. Wang, Z.M. Sun, D. Feng, Effects of high-frequency a.c. electric field on the helical structure in a ferroelectric liquid crystal. Europhys. Lett. **14**(8), 785 (1991)
45. B.S. Srikanta, N.V. Madhusudana, Dielectric relaxation studies on two systems exhibiting the induced smectic A phase. Mol. Cryst. Liq. Cryst. **108**(1–2), 39 (1984)